Background-free nonlinear microspectroscopy with vibrational molecular interferometry

Erik T. Garbacik[a], Jeroen P. Korterik[a], Cees Otto[b], Shaul Mukamel[c], Jennifer L. Herek[a], and Herman L. Offerhaus[a,†]

[a]Optical Sciences group, MESA+ Institute for Nanotechnology, University of Twente, 7500AE Enschede, the Netherlands;
[b]Medical Cell BioPhysics group, MIRA Institute for Biomedical Technology and Technical Medicine, University of Twente, 7500AE Enschede, the Netherlands;
[c]Department of Chemistry, University of California, Irvine, CA 92697, USA

ABSTRACT

We demonstrate a method for performing nonlinear microspectroscopy that provides an intuitive and unified description of the various signal contributions, and allows the direct extraction of the vibrational response. Three optical fields create a pair of Stokes Raman pathways that interfere in the same vibrational state. Frequency modulating one of the fields leads to amplitude modulations on all of the fields. This vibrational molecular interferometry (VMI) technique allows imaging at high speed free of non-resonant background, and is able to distinguish between electronic and vibrational contributions to the total signal.

Keywords: Nonlinear optics, coherent anti-Stokes Raman scattering, spectroscopy, microscopy, dissipative, phase modulation

1. INTRODUCTION

For a number of decades much of the development of new coherent anti-Stokes Raman scattering (CARS) techniques has been focused on suppressing or eliminating the persistent non-resonant background that reduces contrast and can render experiments involving low concentrations of resonant oscillators impossible. Various methods developed so far include exploiting the polarization dependences of the resonant and non-resonant components of $\chi^{(3)}$,[1–5] directly measuring[6–8] or extracting[9–11] the vibrational phase of the oscillators, shaping the phase of a broadband optical pulse to match that of the molecule,[12–15] or introducing temporal delays to probe the resonant vibrational state after the non-resonant coherence has decayed.[16,17]

Recent work by Rahav and Mukamel[18] introduced a new paradigm regarding coherent Raman scattering experiments. Rather than operating in the common semi-classical field perspective, they focus on energy transfer from a molecular quantum mechanical point of view. The semi-classical approach of nonlinear optics assumes classical fields interacting with quantum matter. The detected mode is singled out from the outset and is described using the macroscopic Maxwell's equations. Heterodyne detection is viewed as an interference of the signal field with a local oscillator field, which makes it hard to establish connections between different experiments with the same pulse configuration where different modes are detected. The quantum description of heterodyne-detected four-wave mixing is much more transparent.

2. THEORY

We consider a steady state of the molecule with ground state $|a\rangle$ and vibrational state $|c\rangle$, and four modes of the radiation field ($\omega_1 - \omega_2 = \omega_4 - \omega_3 = \omega_{ca}$, with $\omega_2 < \omega_1$ and $\omega_3 < \omega_4$). The optical field modes are all far detuned from the lowest electronic excited state $|b\rangle$. All modes, including the local oscillator, are treated in the same microscopic way. Heterodyne detection then emerges as a stimulated process involving the detected mode. This

†Address correspondence to Herman Offerhaus: h.l.offerhaus@utwente.nl

Multiphoton Microscopy in the Biomedical Sciences XII, edited by Ammasi Periasamy, Karsten König, Peter T. C. So,
Proc. of SPIE Vol. 8226, 822605 · © 2012 SPIE · CCC code: 1605-7422/12/$18 · doi: 10.1117/12.908158

approach provides a more intuitive and unified description of the various signals and traces their microscopic origins.

The probability for a Raman-active transition from the ground state $|a\rangle$ to a vibrational state $|c\rangle$ is

$$P_{a\to c} = P^{12}_{a\to c} + P^{34}_{a\to c} + P^{1234}_{a\to c}$$

where the terms $P^{12}_{a\to c}$ and $P^{34}_{a\to c}$ are the individual pump-probe (Stokes Raman) processes into the vibrational state. The last term, $P^{1234}_{a\to c}$, is the interference of these two processes that yields the resonant component of the CARS signal, and is associated with the imaginary component of $\chi^{(3)}$. This resonant dissipative term involves energy that is transferred from the optical fields into the molecule. In addition to this dissipative term there is a non-resonant parametric component S^{par} that is equivalent to the real part of $\chi^{(3)}$ in which energy is merely rearranged between the field modes and the molecule returns to the ground state. The parametric and dissipative energy level diagrams are shown in Figs. 1(a) and (b), respectively.

An emission process produces an increase in the intensity of a given field mode, whereas an absorption process results in a decrease in intensity. By tallying the gain and loss contributions from the dissipative and parametric processes for each field mode, we find that the changes in the intensities of the field modes after interacting with a sample are then given by

$$\begin{aligned} S_1 &= -\frac{1}{2}P^{1234}_{a\to c} - S^{\text{par}} \\ S_2 &= +\frac{1}{2}P^{1234}_{a\to c} + S^{\text{par}} \\ S_3 &= +\frac{1}{2}P^{1234}_{a\to c} - S^{\text{par}} \\ S_4 &= -\frac{1}{2}P^{1234}_{a\to c} + S^{\text{par}} \end{aligned}$$

where the factor of 1/2 signifies that only one of the Stokes Raman processes affects the number of photons in each field mode. From these relations it is clear that the parametric contribution may be eliminated by measuring $S_4 - S_2 = -P^{1234}_{a\to c}$, which is the purely dissipative interference term. In this paper we demonstrate the measurement of this purely dissipative signal.

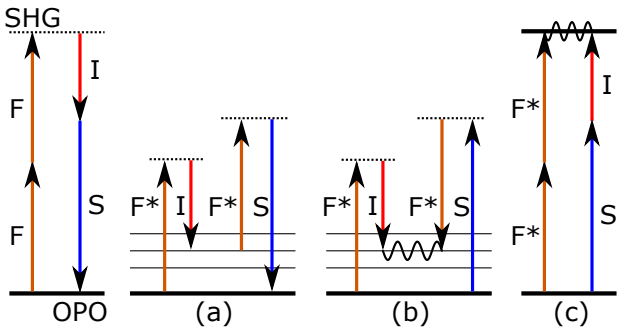

Figure 1. Energy level diagrams of the cascaded phase-preserving chain (left) and (a) parametric, (b) vibrational dissipative, and (c) electronic dissipative energy transfer processes in the molecule. F = laser fundamental at 1064 nm, F* = frequency modulated laser fundamental, S = OPO signal, I = OPO idler. Thick lines are electronic states, thin solid lines are vibrational levels, and dotted lines are virtual states.

The magnitude of the dissipative energy transfer is very small compared to the incident field amplitudes ($\delta I/I < 10^{-4}$). To separate this signal from the large DC background we shift the frequencies of the two Stokes Raman pathways ($1 \to 2$ and $4 \to 3$) relative to each other. The population in the vibrational level is modulated

by the beating of these two pathways, and the modulation carries over onto each of the driving fields as an amplitude fluctuation at the difference frequency. This amplitude modulation is then detected on each field separately using lock-in amplification. Rather than using four independent fields, we synchronously pump an optical parametric oscillator (OPO) with the second harmonic of a 1064-nm laser (see Fig. 1(left)) to generate a pair of frequency-locked beams, the *signal* and *idler*. The frequency of the residual laser fundamental is shifted with an acousto-optic modulator (AOM). All three beams are subsequently mixed in the sample.

The vibrational frequency accessed by the combination of the laser fundamental (S_1) and idler (S_2) is identical to that of the laser fundamental (S_3) and signal (S_4); in the former situation, the laser fundamental is used as a pump beam, while in the latter it functions as the Stokes. Because the laser fundamental is used in opposite ways in the two Stokes Raman processes, the difference frequency between the two pathways is twice the frequency applied to the AOM. All of the beams carry an amplitude modulation at the beat frequency of these two Stokes Raman pathways, and their relative signs indicate whether a net gain or loss is observed: the signal experiences loss and the idler gain, while the gain or loss of the laser fundamental is determined by which Stokes Raman pathway is dominant. In our experiment the signal field is stronger than that of the idler, and so the laser fundamental field carries net gain in the presence of a vibrational state.

Interestingly, electronic states resonant with the two-photon absorption of the laser fundamental second harmonic and the signal-idler sum frequency can also generate the amplitude modulations as described above (Fig. 1(c)). However, the idler and the laser fundamental experience net gain in a vibrational resonance, whereas *all* fields experience net loss in a resonant electronic transition. The difference of the idler (S_2) and signal (S_4) intensities contains no electronic contribution, while the laser fundamental experiences loss in an electronic level and, as stated above, gain in a vibrational level. Monitoring the relative gain and loss of all three beams therefore allows us to distinguish between electronic and vibrational resonances without interference from non-resonant background. We refer to this process as vibrational molecular interferometry, or VMI.

3. EXPERIMENTAL SETUP

The optical setup used for these experiments, shown schematically in Fig. 2, is similar to that described by Jurna *et al.*[19] A frequency-doubled Nd:YVO_4 laser (Coherent Paladin) pumping an optical parametric oscillator (APE Berlin Levante Emerald) generates three frequency- and phase-locked beams. An acousto-optic modulator (AOM) placed in the laser fundamental beam shifts the carrier frequency of that beam by 500 kHz. The three beams are expanded with telescopes, temporally overlapped with delay stages and spatially combined on a pair of dichroic mirrors. The idler is set to be slightly convergent to compensate for chromatic aberration of the focusing objective. Waveplates in each beam are used to align all polarizations along the same direction. The maximum average power on the sample is about 130 mW (80 mW signal, 30 mW laser fundamental, 20 mW idler) and decreases as the OPO is tuned away from its gain optimum.

The beams are laterally scanned with a pair of galvano mirrors (Olympus FluoView300/IX71), focused into the sample with an IR-corrected 1.2 NA water immersion objective (Olympus UPLSAPO), collected in the forward direction with a 0.55 NA long-working-distance objective, and spectrally separated onto individual detectors with dichroic mirrors. The idler beam is detected on a large-area InGaAs photodiode (ThorLabs FGA21), while the laser fundamental and signal beams are each sent to separate large-area silicon diodes (ThorLabs TDS1010). Forward- and backward-scattered CARS and fluorescence emissions are transmitted through spectral bandpass filters centered at the CARS wavelength and detected on photomultiplier tubes (Hamamatsu R3986). The outputs of all four forward detectors are sent to a pair of high-frequency lock-in amplifiers (Zurich Instruments HF2-LI) set to demodulate the second harmonic of the modulation frequency on the laser fundamental.

4. RESULTS

4.1 Microscopy

For microscopy on a sample of mayonnaise the output of the OPO is fixed to probe the symmetric CH_2 stretch at 2845 cm^{-1} (λ_s = 816.8 nm, λ_i = 1526 nm), and the beams are raster scanned across the sample. An image containing 256 × 256 pixels is acquired without averaging in about 4 seconds with a 25-μs lock-in time constant. The amplitudes of the signal and idler channels are corrected for differences in the spectral responses

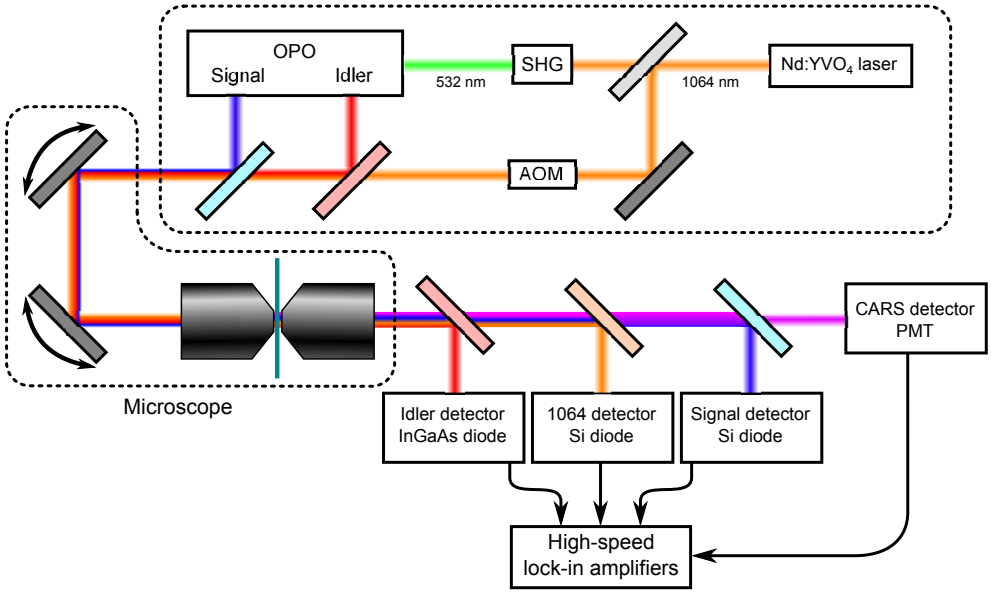

Figure 2. Optical setup used in this experiment. OPO: optical parametric oscillator; SHG: second-harmonic generation; AOM: acousto-optic modulator; PMT: photomultiplier tube. Delay lines, polarization control optics, and telescopes are not shown.

of the detectors, scaled to account for the lock-in detector settings, and subtracted from each other ($S_4 - S_2$) to produce a background-free image in real time. Figure 3 demonstrates the comparison of forward-detected CARS, background-free vibrational phase contrast (VPC) CARS,[19] and VMI. A strong non-resonant background from water in the sample significantly reduces contrast in the F-CARS image, but is absent in both the VPC-CARS and VMI images. Differences between the VMI and VPC-CARS images are attributed to the lack of a phase-matching condition in the former.[18]

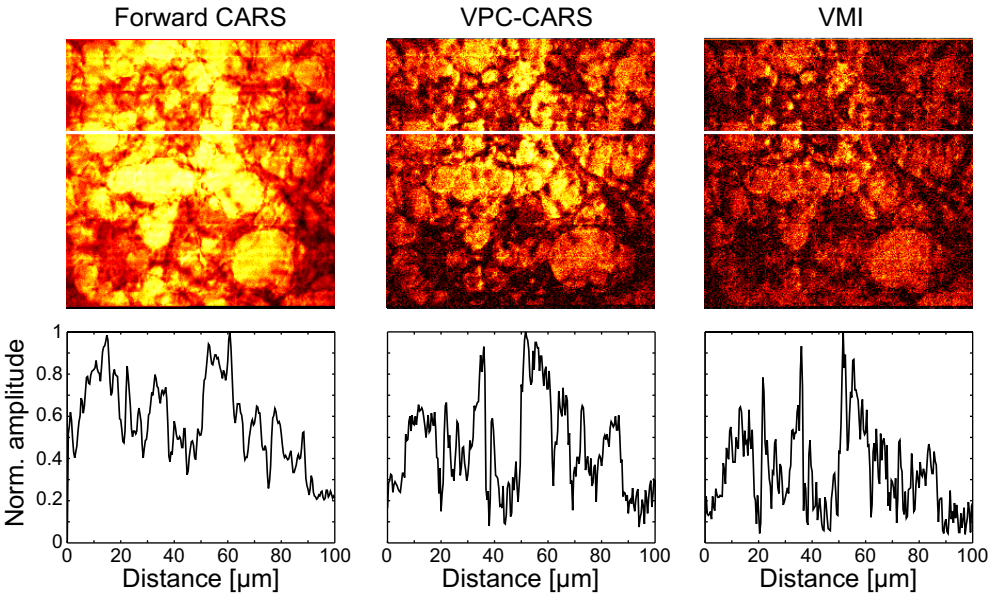

Figure 3. Mayonnaise images at 2845 cm^{-1} with CARS (left), VPC-CARS (center), and VMI (right), with intensity plots at the indicated line shown below.

4.2 Vibrational spectroscopy

Background-free spectroscopy with VMI is demonstrated in the alkyl region on a sample of neat DMSO, and compared to CARS and VPC-CARS spectra in Fig. 4. The overall agreement between the two background-free techniques is good over most of the spectrum. In particular, the features of the CARS spectrum arising from the non-resonant background—a shift of the main peak (nominally 2915 cm^{-1}) to a lower frequency (2912 cm^{-1}), marked asymmetry of that prominent peak, and a skewed ratio of heights of the 2915-cm^{-1} and 3000-cm^{-1} peaks—are noticeably absent in both the VPC-CARS and VMI spectra. Low optical power on the edge of the OPO gain curve contributes to noise in the VMI measurement that manifests as an offset between the VMI and VPC-CARS spectra below 2905 cm^{-1}. This artifact does not appear in the VMI measurement shown in Fig. 5(b).

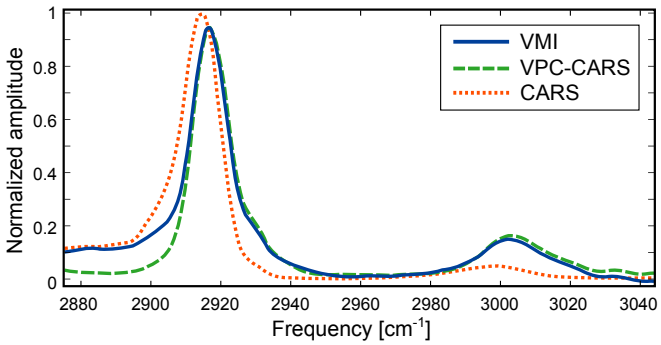

Figure 4. Vibrational spectrum of neat DMSO measured with CARS, VPC-CARS, and VMI. All spectra have been corrected for changes in optical power. Note that the CARS signal is actually an intensity rather than an amplitude.

4.3 Electrovibrational spectroscopy

Electronically resonant processes can present problems for CARS and spontaneous Raman scattering measurements because of fluorescent emissions. As a model example of a problematic system, we use DCM-pyran, a laser dye which has a broad absorption band covering most two-photon resonances of the wavelengths used in this experiment, and an emission maximum near the CARS wavelength (see Fig. 5(a) for spectra).[20] The emission spectrum from a saturated solution of DCM-pyran in DMSO is dominated by fluorescence, masking the strong 2912-cm^{-1} resonance in the backward-scattered CARS signal, as shown in Fig. 5(b). However, the VMI spectrum (signal minus idler) clearly shows the background-free DMSO peak with only a minor residual contribution from the DCM-pyran. Furthermore, the modulation detected on the laser fundamental (labeled "1064 nm" in Fig. 5(b)) shows net loss from the electronic DCM-pyran contribution away from the DMSO resonance, and a positive peak at the DMSO resonance.

5. CONCLUSION

In summary, we have demonstrated a new quantum mechanical approach for nonlinear microspectroscopy that exploits interference between two competing Stokes Raman pathways in analogy to coherent control.[21,22] Wave mixing techniques such as CARS which only detect a single beam contain non-dissipative (parametric) contributions that reflect energy exchange between field modes and add undesired, matter-independent background. However, with this more elaborate detection of all modes we have shown that it is possible to convert CARS into a fully dissipative technique. Compared to the more practical technique of stimulated Raman scattering (SRS), VMI has the potential to provide more insights at the cost of technical complexity. For example, the vibrational phase can be retrieved (not shown here) so that mixtures with overlapping resonances can be analyzed.[8] The use of properly phased broadband pulses, akin to femtosecond stimulated Raman scattering (FSRS) techniques,[23,24] would produce stronger signals than are currently obtained in narrowband VMI.[25]

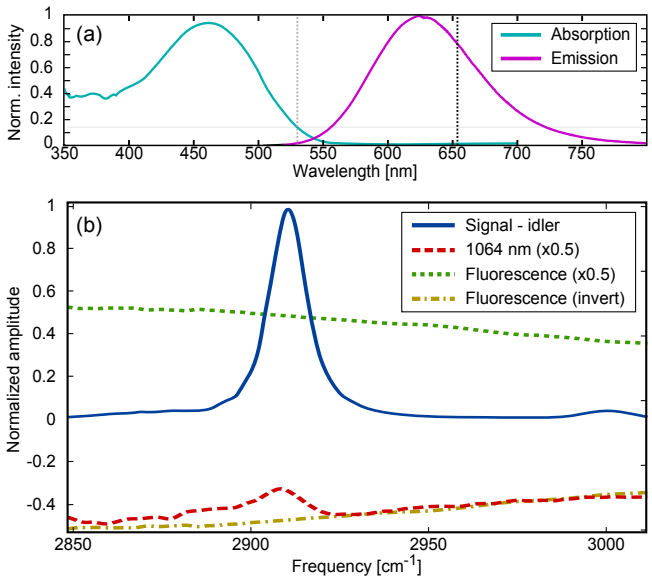

Figure 5. (a) Electronic spectrum of DCM-pyran. The vertical lines indicate (left) the SHG of the laser fundamental and SFG of the idler and signal and (right) the CARS wavelength. (b) Simultaneous background-free vibrational and electronic measurements of DMSO saturated with DCM-pyran. Inverting the fluorescence measurement associates it with an absorptive (loss) process, corresponding to the physical mechanism affecting the 1064-nm curve. None of the spectra have been corrected for optical power so as to illustrate the agreement between the fluorescence and 1064-nm profiles.

ACKNOWLEDGMENTS

We are grateful for many useful discussions with Alexander van Rhijn, Dr. Chris Lee, and Dr. Pepijn Pinkse. Partial funding is provided by the Stichting voor Fundamenteel Onderzoek der Materie (FOM), and by a VICI grant to JLH from the Nederlandse Organisatie voor Wetenschappelijk Onderzoek (NWO). SM gratefully acknowledges the support of the National Institutes of Health (Grant GM059230 and GM091364), NSF grant CHE-1058791, and DARPA BAA-10-40 QUBE. We further thank Coherent Inc. for use of the Paladin laser, and APE Berlin for the Levante Emerald OPO.

REFERENCES

1. Akhmanov, S. A., Bunkin, A. F., Ivanov, S. G., and Koroteev, N. I., "Coherent ellipsometry of Raman scattering of light," *JETP Lett.* **25**, 416 (1977).
2. Chikishev, A., Lucassen, G., Koroteev, N., Otto, C., and Greve, J., "Polarization sensitive coherent anti-Stokes Raman scattering spectroscopy of the amide I band of proteins in solutions," *Biophys. J.* **63**, 976–985 (October 1992).
3. Lucassen, G., *Polarization sensitive coherent Raman spectroscopy on (bio)molecules in solutions*, PhD thesis, University of Twente (1992).
4. Cheng, J.-X., Book, L. D., and Xie, X. S., "Polarization coherent anti-Stokes Raman scattering microscopy," *Opt. Lett.* **26**(17), 1341–1343 (2001).
5. Orsel, K., Garbacik, E. T., Jurna, M., Korterik, J. P., Otto, C., Herek, J. L., and Offerhaus, H. L., "Heterodyne interferometric polarization coherent anti-Stokes Raman scattering (HIP-CARS) spectroscopy," *J. Raman Spectrosc.* **41**(12), 1678–1681 (2010).
6. Potma, E. O., Evans, C. L., and Xie, X. S., "Heterodyne coherent anti-Stokes Raman scattering (CARS) imaging," *Opt. Lett.* **31**(2), 241–243 (2006).
7. Jurna, M., Korterik, J. P., Otto, C., Herek, J. L., and Offerhaus, H. L., "Background free CARS imaging by phase sensitive heterodyne CARS," *Opt. Express* **16**(20), 15863–15869 (2008).

8. Jurna, M., Garbacik, E. T., Korterik, J. P., Herek, J. L., Otto, C., and Offerhaus, H. L., "Visualizing resonances in the complex plane with vibrational phase contrast CARS," *Anal. Chem.* **82**(16), 7656–7659 (2010).
9. Rinia, H. A., Bonn, M., Mller, M., and Vartiainen, E. M., "Quantitative CARS spectroscopy using the maximum entropy method: The main lipid phase transition," *Chem. Phys. Chem.* **8**(2), 279–287 (2007).
10. Chimento, P. F., Jurna, M., Bouwmans, H. S. P., Garbacik, E. T., Hartsuiker, L., Otto, C., Herek, J. L., and Offerhaus, H. L., "High-resolution narrowband CARS spectroscopy in the spectral fingerprint region," *J. Raman Spectrosc.* (2009).
11. Liu, Y., Lee, Y. J., and Cicerone, M. T., "Broadband CARS spectral phase retrieval using a time-domain Kramers-Kronig transform," *Opt. Lett.* **34**, 1363–1365 (May 2009).
12. Oron, D., Dudovich, N., Yelin, D., and Silberberg, Y., "Quantum control of coherent anti-Stokes Raman processes," *Phys. Rev. A* **65**, 043408 (2002).
13. Lim, S.-H., Caster, A. G., and Leone, S. R., "Single-pulse phase-control interferometric coherent anti-Stokes raman scattering spectroscopy," *Phys. Rev. A* **72**, 041803 (Oct 2005).
14. Postma, S., van Rhijn, A. C. W., Korterik, J. P., Gross, P., Herek, J. L., and Offerhaus, H. L., "Application of spectral phase shaping to high resolution CARS spectroscopy," *Opt. Express* **16**, 7985–7996 (May 2008).
15. van Rhijn, A. C. W., Offerhaus, H. L., van der Walle, P., Herek, J. L., and Jafarpour, A., "Exploring, tailoring, and traversing the solution landscape of a phase-shaped CARS process," *Opt. Express* **18**(3), 2695–2709 (2010).
16. Volkmer, A., Book, L. D., and Xie, X. S., "Time-resolved coherent anti-Stokes Raman scattering microscopy: Imaging based on Raman free induction decay," *Appl. Phys. Lett.* **80**, 1505–1507 (2002).
17. Selm, R., Winterhalder, M., Zumbusch, A., Krauss, G., Hanke, T., Sell, A., and Leitenstorfer, A., "Ultrabroadband background-free coherent anti-Stokes Raman scattering microscopy based on a compact Er:fiber laser system," *Opt. Lett.* **35**, 3282–3284 (Oct 2010).
18. Rahav, S. and Mukamel, S., "Stimulated coherent anti-Stokes Raman spectroscopy (CARS) resonances originate from double-slit interference of two-photon Stokes pathways," *Proc. Natl. Acad. Sci. U. S. A.* **107**, 4825–4829 (January 2010).
19. Jurna, M., Korterik, J. P., Otto, C., Herek, J. L., and Offerhaus, H. L., "Vibrational phase contrast microscopy by use of coherent anti-Stokes Raman scattering," *Phys. Rev. Lett.* **103**, 043905–(1–3) (2009).
20. Du, H., Fuh, R. A., Li, J., Corkan, A., and Lindsey, J. S., "Photochemcad: A computer-aided design and research tool in photochemistry," *Photochem. Photobio.* **68**, 141–142 (1998).
21. Glauber, R. J., "Coherent and incoherent states of the radiation field," *Phys. Rev.* **131**, 2766–2788 (1963).
22. Brumer, P. and Shapiro, M., "Laser control of molecular processes," *Ann. Rev. Phys. Chem.* **43**, 257–282 (1992).
23. Frostig, H., Katz, O., Natan, A., and Silberberg, Y., "Single-pulse stimulated Raman scattering spectroscopy," *Opt. Lett.* **36**, 1248–1250 (Apr 2011).
24. Ploetz, E., Marx, B., and Gilch, P., "Origin of spectral interferences in femtosecond stimulated Raman microscopy," *J. Raman Spectrosc.* (2011).
25. Zhang, D., Slipchenko, M., and Cheng, J.-X., "Highly sensitive vibrational imaging by femtosecond pulse stimulated Raman loss," *J. Phys. Chem. Lett.* **2**, 1248–1253 (2011).